

State-of-the-Art High Power Density and High Efficiency DC-DC Chopper Circuits for HEV and FCEV Applications

Atsuo Kawamura, Martin Pavlovsky, Yukinori Tsuruta

Yokohama National University/ Electrical and Computer Engineering, Yokohama, Japan, e-mail: *kawamura@ynu.ac.jp*

Abstract— recent environmental issues have accelerated the use of more efficient and energy saving technologies in any area of our daily life. One of the major energy consumptions is in the transportation area, especially in the automobile field. DC/DC chopper circuits for use in hybrid electric vehicles (HEV), fuel cell electric vehicles (FCEV) and so on will be discussed in this paper from the view point of power density and efficiency. A typical power range of such converters can be in order of kW up to over 100 kW with a short term overload requirement of often more than 200 %. Considering the state of the art, switching frequency of these converters is in the range from 50 kHz with IGBTs to 200 kHz with power MOSFETs, the power density peaks at about 25 kW/l, and the highest efficiency is close to 98 [%] depending on the load conditions. As can be seen from the brief introduction, the design of such converter presents multiple challenges from power density as well as efficiency point of view and these are discussed further in the paper.

I. INTRODUCTION

Recent global environmental issues have accelerated the use of more efficient and energy saving technologies in many areas of daily life. Major energy consumptions is the transportation, especially the automobile field. The need of more efficient use of internal combustion engine (ICE) and for an improvement of total system efficiency has created a combination of ICE and electric motors i.e. hybrid electric vehicles (HEV). Even pure electric vehicles (EV) and fuel cell electric vehicles (FCEV) could be commercially available soon. The need of DC/DC choppers is discussed for these electric power trains [1]-[9]. The advantage of DC/DC chopper for HEV is: 1) higher power output in a high speed range [1], and 2) total efficiency increase. FCEV and Pure EV may need a very high efficiency chopper for the higher performance of power-train characteristics [2],[3]-[4].

The power rating of DC/DC choppers for HEV lies in the range between 30 and 90 kW, and it may be beyond 100 kW for EV and FCEV. The main design target points are often high power density and high efficiency. There is few literature available considering this power range and a new performance criterion should be applied. Ohashi proposed the new concept of "Power density" [5] and [6], and he showed the trend of the continuous growth of power density in various applications of power electronics. Kolar in [7] listed four key items which strongly influence final converter design, which are:

- efficiency (loss)
- volume
- weight
- cost

These items are closely coupled together and the total optimisation procedure is discussed in [7].

In this paper, several examples of high power density and high efficiency DC/DC choppers for FCEV and EV will be introduced. They are based on so called SAZZ topology (Snubber assisted zero-voltage-zero-current transition switch) which offers soft switching at turn-on as well as at turn-off in order to reduce the switching losses [23], [24]. The considered power range is 8 to 25 kW with the switching frequency up to 100 kHz with IGBTs and 200 kHz with MOSFETs respectively. The main goal of the presented designs is reaching as high power density and efficiency as possible. The presented converter prototypes exhibit power density as high as 25 kW/l and efficiency close to 98 %.

In the following paragraphs, analyses of several SAZZ based circuit topologies with the main goal being the highest efficiency will be discussed followed by review of various issues related to reaching high power density.

II. HIGH EFFICIENCY

A. Review of Highly Efficient converter topologies

Switching power supplies and regulators have come into widespread use since 1970s. Basic high switching frequency converter design is shown in Figure 1(a) as published in [11], [12]. This circuit based on basic hard-switching buck/boost topology reached the operating frequency limit in the 1980s. In order to increase the frequency further and hence improve the power density, soft switching with one resonant switch as shown in Figure 1(b) was proposed in [13]. However, excessive current and voltage spikes in the switching devices are pointed out as the drawback. A solution to this problem was proposed in [12], [15] as ZVT (Zero Voltage Transition) circuit topology with two switches as shown in Figure 1(c) This partial resonance topology became the basic soft switching topology and various applications were proposed in the literature. Our literature survey showed that boost choppers are mostly based on one resonant switch [13] as shown in Figure 1(b), passive auxiliary resonant circuit [16] (with added passive snubber) as shown in Figure 1(d) and ZVT [15]. In case of high booster ratio, the most used topology is based on coupled inductors [17] as shown in Figure 1(e). However, most of the surveyed papers were in the power range below 1 kW. There are very few examples of papers regarding 100 kW range for EV application with the exception being the non-isolated bidirectional converter discussed in [18] and shown in Figure 1(d).

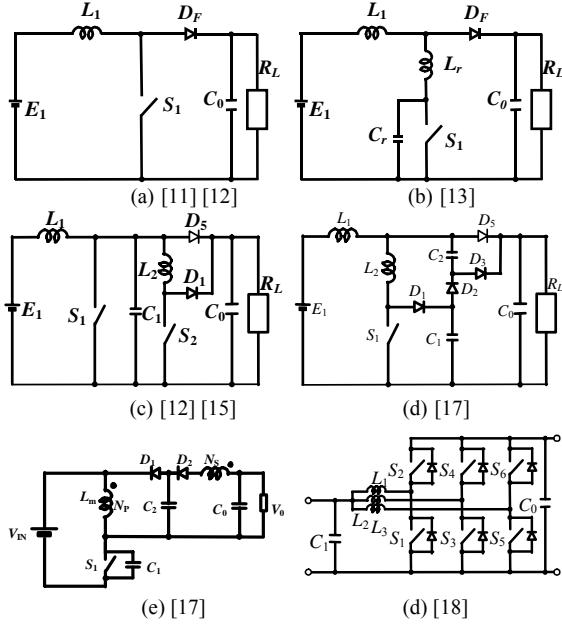


Figure 1: High efficiency switching topologies

B. Proposal of New High Efficiency Chopper Circuits

This paragraph discusses the recent author's effort and research activities in improving the efficiency of high power bi-directional chopper circuits.

C-Bridge switch shown in Figure 2(a) was proposed in [19] for high power application (8 kW) and 96.0 % efficiency at 25 kHz was obtained. Later on, Quasi-resonant Regenerating Active Snubber (QRAS) was proposed in [20] to achieve ZCS turn-on and ZVS turn-off and regenerating the snubber energy. The efficiency of 97.5 % was obtained for an 8 kW prototype operating at 25 kHz. The efficiency was further improved by using new semiconductor devices. This was published in [21] [22] where efficiency improvement from 97.5 % to 98.5 % operating again at 25 kHz was reported. The improvement was achieved by using SiC schottky diodes in 8 kW QRAS chopper. SAZZ (Snubber Assisted Zero Voltage and Zero Current Transition) topology was proposed after reconsidering the QRAS soft switching operation. SAZZ implements ZVZCT turn-on and ZVS turn-off while using fewer circuit components, than in QRAS topology [23]. 97.8 % efficiency was measured on SAZZ converter prototype operating at 100 kHz with the power output of 8 kW [24]. The SAZZ circuit operational principle was extended to a bidirectional buck and boost SAZZ chopper circuit in [25]. The bi-directional converter was tested as a 25 kW converter prototype operating at 50 kHz. The topology reached 96.6 % efficiency in boost mode and 97.4 % in buck mode under nominal power output of 25 kW. The presented topologies are discussed in more details in the following paragraphs with the main goal being high efficiency. As shown further, the proposed topologies offer high-efficiency for high-power applications. The prototypes discussed below were mostly constructed as scaled down models with further power increase kept in mind. The prototypes were tested at rated conditions, under light load, discontinuous current mode and out of resonance operation.

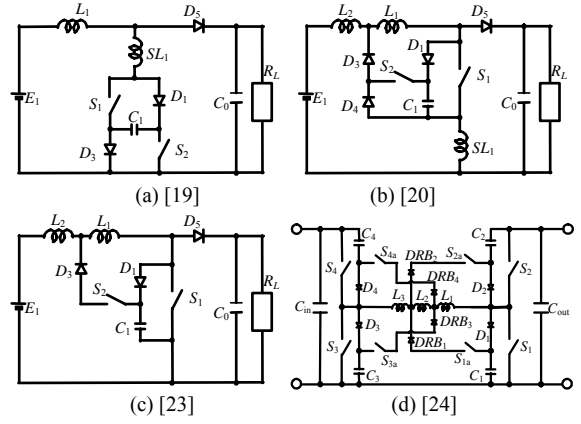


Figure 2: New high efficiency switching topologies

C. QRAS Chopper Circuit (25 kHz, 8 kW) [20]

Figure 3 depicts the circuit diagram of QRAS DC-DC chopper. The main parts of the proposed topology are: two switches (S_1 and S_2), three diodes (D_1, D_3 and D_4) and a capacitor C_2 . This configuration retains the desirable properties of the low turn on loss and low turn off loss by so called "soft switching". Figure 4 shows basic operating waveforms of the QRAS chopper where as Figure 5 depicts the corresponding operational modes. When the switch S_1 turns on, the current rise through the switch is limited by the additional inductor S_{L1} (Mode2 in Figure 4 and in Figure 5(b)). On the other hand, when switch S_1 is turned off, the voltage rise across the switch is limited by the snubber capacitor C_2 (Mode5 in Figure 4 and in Figure 5(e)). Thus, the converter uses a loss less snubber and high efficiency operation can be achieved.

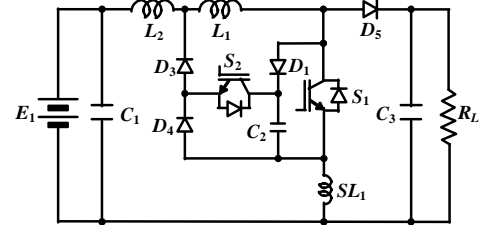


Figure 3: Circuit configuration of the QRAS chopper

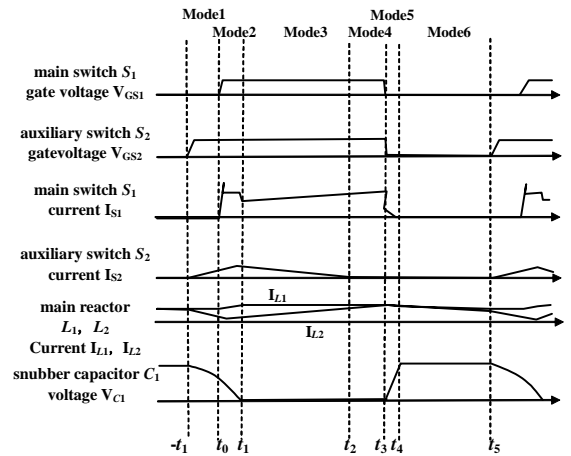


Figure 4: Operating waveforms of the QRAS chopper

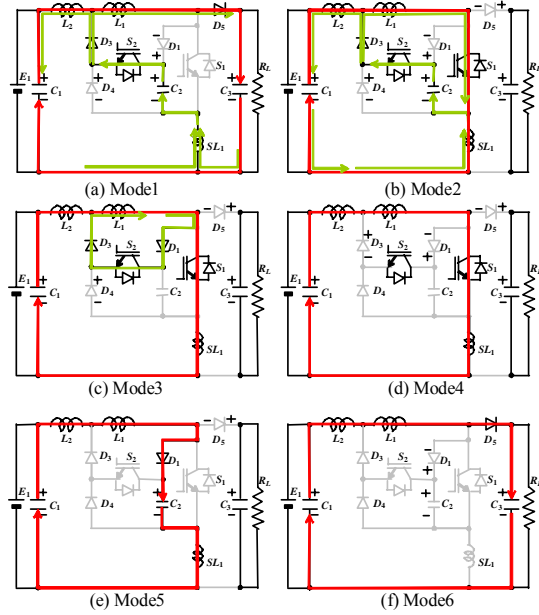


Figure 5: Six operational modes of QRAS chopper.

The soft switching area of QRAS chopper is shown in Figure 6. In almost whole boost operational region, ZCS turn-on and ZVS turn-off can be achieved. 8 kW prototype-model using IGBTs was made as shown in Figure 7. The prototype specifications are listed in Table I. Fig.8 shows the main switch voltage and current waveforms.

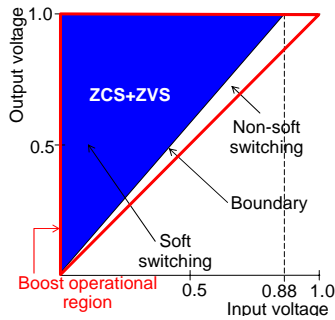


Figure 6: Soft switching area of QRAS topology boost operation

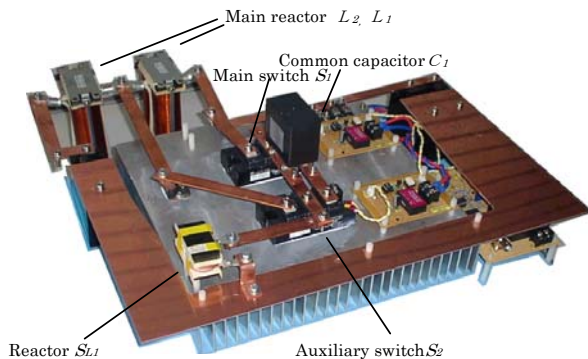


Figure 7: 25 kHz-8 kW QRAS prototype

TABLE I.

SPECIFICATIONS OF 8 kW QRAS PROTOTYPE

Rating	$V_0=400\text{ V}$, $P_{OUT}=8\text{ kW}$
Switch	PDMB100B12C, 1200 V, 100 A
Frequency	25 kHz
Circuit type	QRAS
Control	Pulse width control with open loop
Cooling	Natural air cooling

In order to eliminate the reverse recovery of the output diode D_5 , Si diode was replaced by four paralleled SiC schottky diodes (CSD1012D,1200 V-10 A). The efficiency improvement was evaluated by practical measurements. Figure 9 shows the comparison of converter efficiencies with SiC and with conventional Si diodes for the power output ranging from 1 kW to 8 kW. As can be seen, the observed efficiency improvement is in order of 1 %. The efficiency of 98.5 % was measured at full power output of 8 kW. Measurement of power loss break down showed that the S_1 turn on loss and D_5 turn off loss was reduced by using SiC diodes.

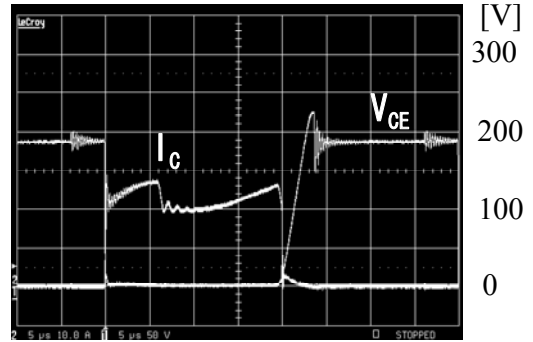


Figure 8: Main switch S_1 voltage and current waveforms; S_1 (PDMB100B12C,1200V,100A)

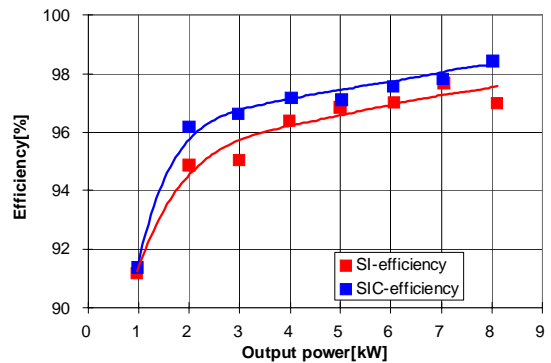


Figure 9: QRAS efficiency measurement results at 400 V output

D. SAZZ Chopper Circuit (100 kHz, 8 kW) [23]

The SAZZ chopper circuit is shown in Figure 10. The main part of the proposed topology includes: two switches (S_1 and S_2), two diodes (D_1 and D_5) and the capacitor C_2 .

The topology offers zero voltage and zero current transition (ZVZCT) turn-on and zero voltage switching (ZVS) turn-off of the main switch S_1 . Figure 11 depicts the basic steady-state voltage and current waveforms where as operating modes are shown in Figure 12.

Prior to turning on the main switch S_1 (at t_0 in Figure 11), the voltage across capacitor C_2 is discharged by the action of the auxiliary switch S_2 (Mode2 in Figure 12 (b)), resulting in zero voltage and zero current in the main switch S_1 . As can be seen, capacitor C_2 is discharged by a resonance with L_2 when switch S_2 turns on (Mode2 in Figure 12). When the switch S_1 is turned off (at t_2 in Figure 11), the voltage across S_1 is snubbed by the capacitor C_2 (Mode5 in Figure 12). The main soft switching area is shown in Figure 13. In almost whole of the boost operational region ZVZCT turn on and ZVS turn off can be achieved. Non-soft switching area depends on the output power. If full discharge condition of the capacitor C_2 is not satisfied with respect to the output power, partial hard switching turn-on and ZVS turn-off are obtained in non-soft switching area [27].

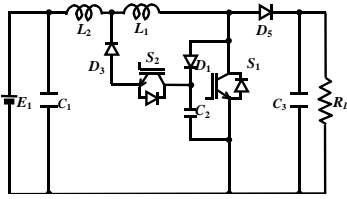


Figure 10: Circuit configuration of the SAZZ chopper

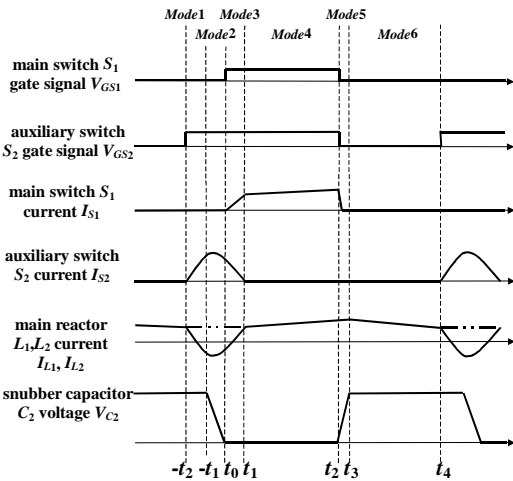


Figure 11: Operating waveforms of the SAZZ chopper.

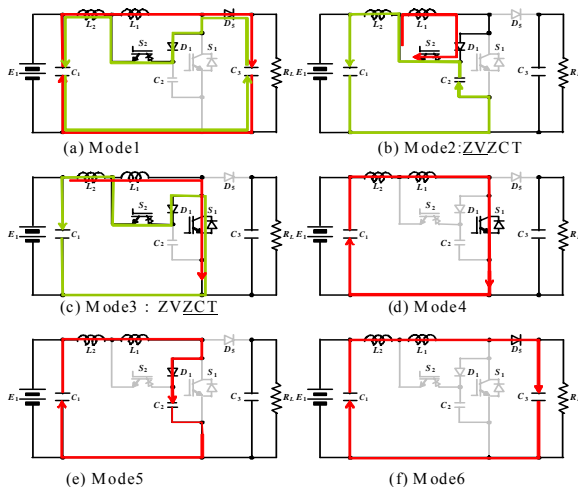


Figure 12: Six operational modes of SAZZ chopper.

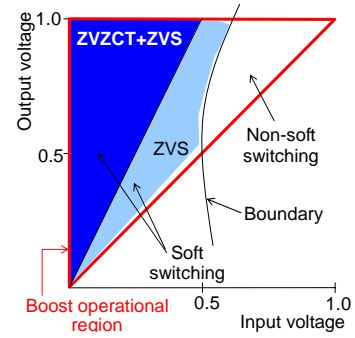


Figure 13: Soft switching area of SAZZ topology, boost operation

100 kHz-8 kW prototype using IGBTs was fabricated as shown in Fig.14. The specification of this prototype-model is listed in Table II. The waveforms measured on the SAZZ prototype are shown in Figure 15. The waveforms confirm that the main switch turns on in ZVZCT mode. The converter efficiency was measured by using HIOKI 3193 POWER HiTESTER. The measured efficiencies for the complete load range are shown in Figure 16. As can be seen, the efficiency of 97.8 % was measured at the full output power of 8 kW and operating frequency of 100 kHz. Table III shows the comparison between SPICE, SiC-SAZZ and SiC-QRAS chopper. As can be seen in Table III, SAZZ topology retains high efficiency of 97.0 % even at the increased operating frequency of 100 kHz. Total reactor loss was reduced from 49.96 W to 15.74 W due to the difference of the topology. However, D_3 loss increased due to the high resonant current (13.9 W to 63.2 W). S_1 turn off loss increased due to the increased higher operating frequency (30 W to 48.8W).

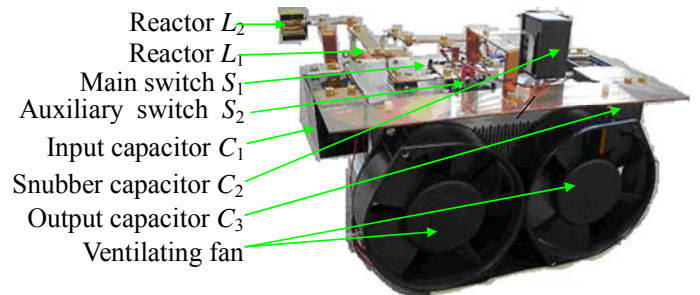


Figure 14: 100 kHz-8 kW SAZZ prototype

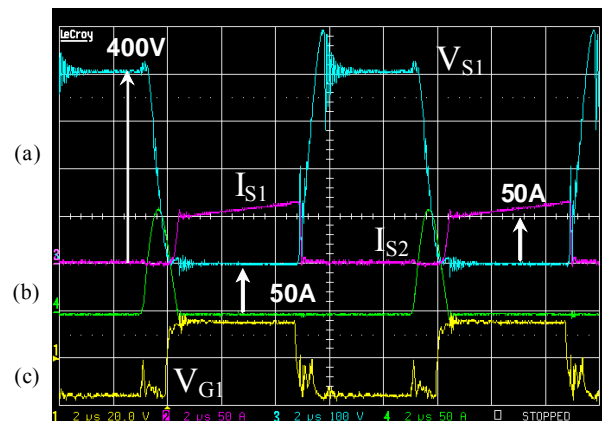


Figure 15: Measured waveforms of SAZZ operation (output=400 V,100 kHz, 8 kW); (a) Main switch S_1 voltage, current (50MT060WH, 600V, 50A), (b) Auxiliary switch S_2 current, (c) Main switch S_1 gate V_{GI}

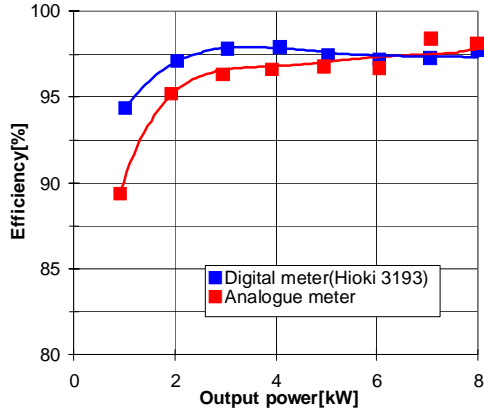


Figure 16: Efficiency curve of SAZZ prototype, 400 V output, 100 kHz.

TABLE II. SPECIFICATIONS OF 8 kW SAZZ PROTOTYPE

Rating	$V_0=400$ V, $P_{OUT}=8$ kW
Switch	50MT060WH, 600 V, 50 A
Frequency	100 kHz
Circuit type	SZZ
Control	Pulse width control with open loop
Cooling	With ventilating fans

TABLE III. 100 kHz-8 kW SiC-SAZZ v.s.25 kHz-8 kW SiC-QRAS LOSS BREAKDOWN.

loss factor	SPICE[W]		100 kHz SiC*-SAZZ[W]		25 kHz SiC*-QRAS [W]	
	SAZZ breakdown	Measured by meter	Measured by breakdown	Measured by meter	Measured by breakdown	Measured by meter
S_1 on-state	60.8		28.9		25.5	
S_1 turn-on	0		6.2		5	
S_1 turn-off	152.7		48.8		30	
S_2 on-state	24.1		24.0		6.5	
S_2 turn-on	0		0		0	
S_2 turn-off	1.7		0		0	
D_1 on-state	14.9		11.5		12.5	
D_1 turn-on	0		0		0	
D_1 turn-off	0		12.2		0	
D_3 on-state	16.2		31.6		13.9	
D_3 turn-on	0		0		0	
D_3 turn-off	5.2		31.6		0	
D_4 on-state					0.2	
D_4 turn-on					0	
D_4 turn-off					0	
D_5 on-state	35		34.9		39	
D_5 turn-on	0		0		9	
D_5 turn-off	0		0		0	
Reactor L_1			13.5		24.5	
Reactor L_2			2.24		24.5	
Reactor SL_1					0.96	
Input power[W]	8109.4	8319		8182		
Output power[W]	7872.5	8079		8049		
Efficiency[%]	97.0	97.1	97.0	98.5	97.6	
Total loss[W]	310.6	240	245.4	133	191.6	

* Output diode D_1 is SiC schottky diode (CSD1012D,1200V-10A×4P) for QRAS, and SiC schottky diode (CSD20060,600V-20A×3P) for SAZZ

E. Bidirectional SAZZ Chopper Circuit (50 kHz, 25 kW) [25]

SZZ circuit operational principle can be extended to a bidirectional buck and boost SAZZ circuit. Such topology created by combining two basic SZZ circuits is shown in Figure 17. Waveforms in the boost-operating mode in forward direction are shown in Figure 18. The six operational modes of the forward buck and boost are shown in Figure 19 and Figure 20. The main soft switching areas are shown in Figure 21 and Figure 22. In almost whole boost operational region and buck operational region as well, ZVZCT turn on and ZVS turn

off can be achieved. Non-soft switching area depends on the output power. In both directions, non-soft switching areas appear due to the boundary condition unsatisfying the snubber capacitor full discharge condition [27]. If full discharge condition is satisfied with respect to the output power, partial hard switching turn on and ZVS turn off are obtained in both non-soft switching areas.

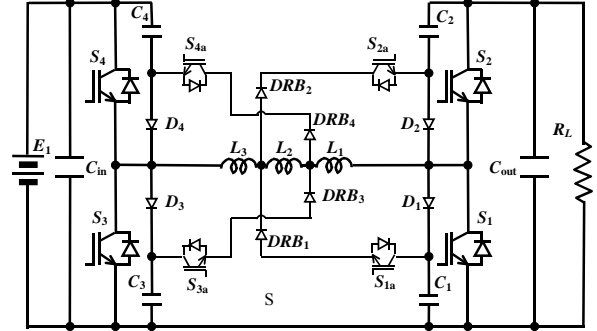


Figure 17: Bidirectional boost and buck SAZZ chopper

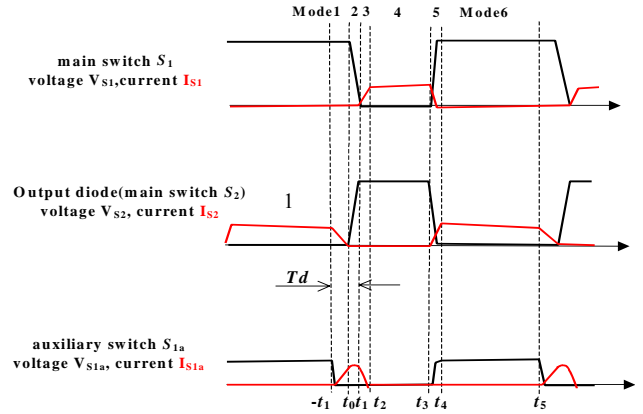


Figure 18: Boost mode operating waveforms of bidirectional SAZZ topology, forward direction.

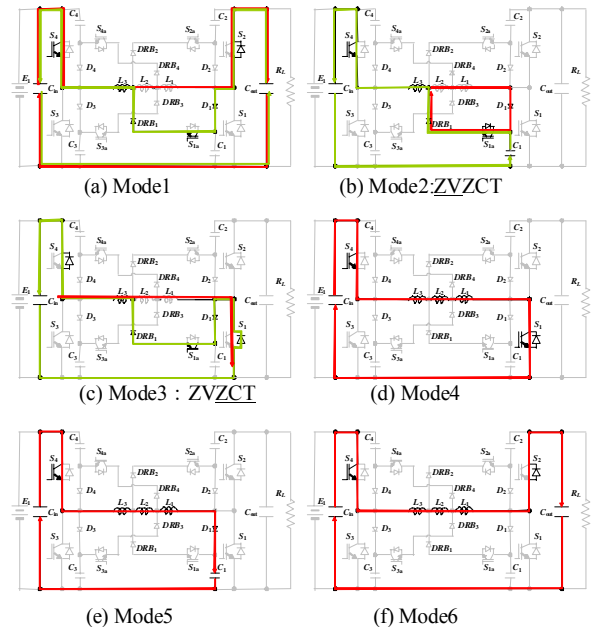


Figure 19: Six operational modes of the forward boost.

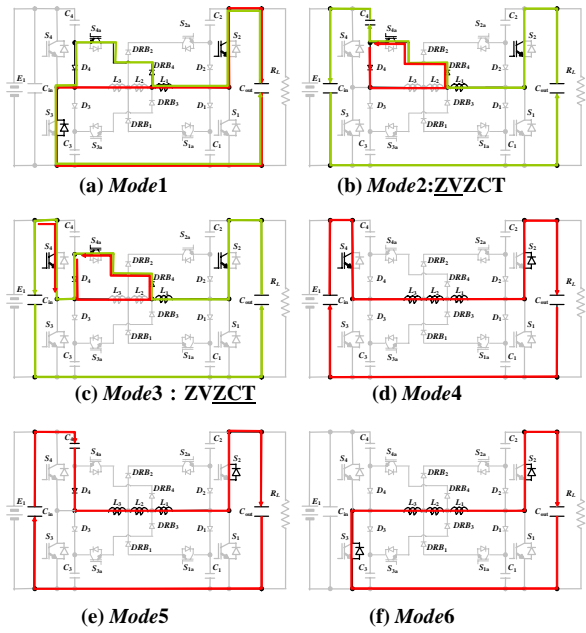


Figure 20: Six operational modes of the forward buck.

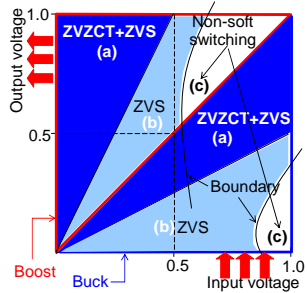


Figure 21: Soft switching area of SAZZ Bidirectional topology (Forward buck and boost operational region).

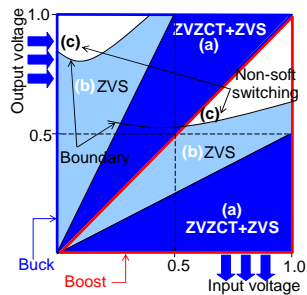


Figure 22: Soft switching area of SAZZ Bidirectional topology (Reverse buck and boost operational region)

Figure 23 and Figure 24 show the efficiency for forward boost operation respectively forward buck operation. Test facilities in the laboratory limited the load condition for boost mode and buck mode operation. Therefore, the efficiency could not be measured under the same input/output voltage condition. The measurements were performed at the load points that were allowed by the load-resistance. It can be concluded that in general the efficiency is higher for buck operation than boost. It is considered that input/output voltage ratio was more suitable for soft switching in buck operation as shown by the comparison of turn-on waveforms between Figure 25 and Figure 26.

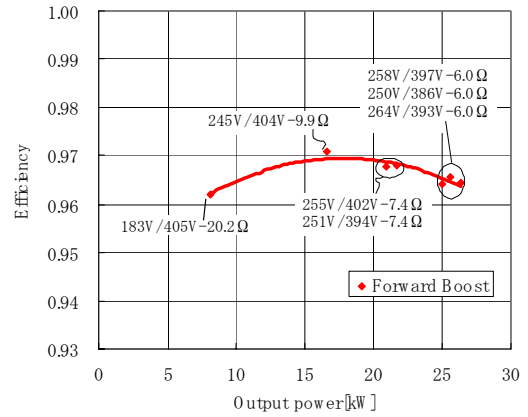


Figure 23: Efficiency of bidirectional SAZZ for forward boost operation

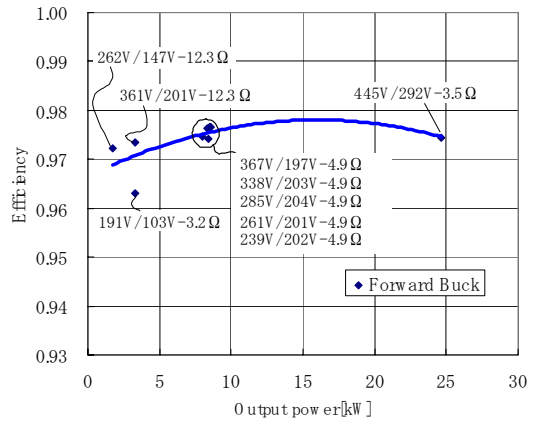


Figure 24: Efficiency of bidirectional SAZZ for forward buck operation

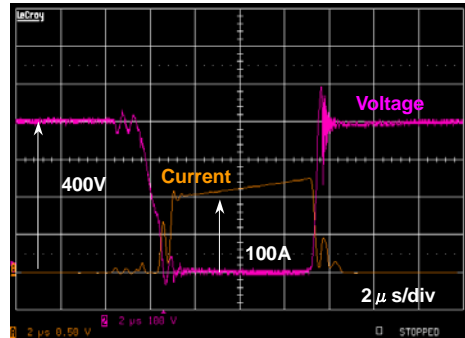


Figure 25: Voltage and current waveforms of the main switch, S_1 (CM200DU-12NFH, 600V, 200A), forward boost mode at 50 kHz-25 kW, 250 V/400 V

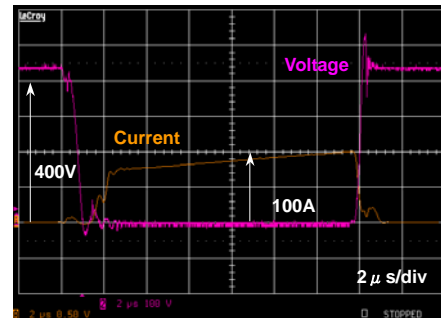


Figure 26: Voltage and current waveforms of the main switch, S_1 (CM200DU-12NFH, 600V, 200A), forward buck mode at 50 kHz-25 kW, 420 V/300 V.

F. High Power 3-Phase Interleaved Boost Chopper Circuit (90kW, 30 kHz)

High power motor drives of FCEV application require high power in the range of 100 kW. Three-phase interleaved boost chopper which operates at 90 kW-30 kHz was developed. Operating frequency of 30 kHz could be reached by implementing SAZZ topology where as conventional hard switching topologies have difficulties to operate over 10 kHz. Figure 27 shows the circuit diagram of the converter. Each phase is phase shifted by 120° with respect to each other. The specifications are defined as follows:

- Operating frequency : 30 kHz
- Output capacity : 90 kW
- Switch : CM600DU24NFH, 1200V, 600A
- Cooling : water cooling

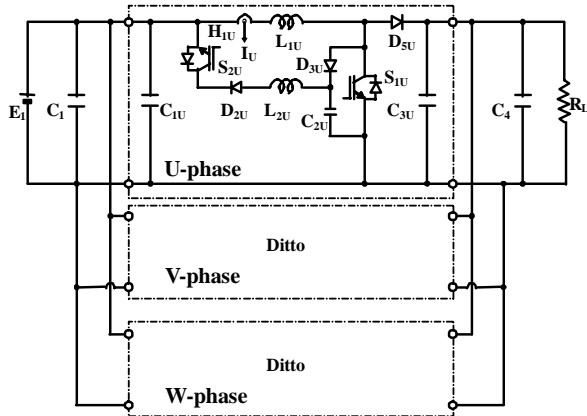


Figure 27: 3-phase interleaved boost chopper.

Figure 28 to Figure 30 show the examples of the waveforms measured on a single phase at 17 kW. The measurements were conducted on per-phase basis due to limit power available in the laboratory. Figure 31 depicts the efficiency characteristics vs. output power. As can be seen, the DC to DC conversion efficiency is more than 95 % and for power levels lower than 8kW it even exceeds 97 %. Figure 32 shows the converter loss breakdown. Total power dissipation consists of main power devices, S1 and D5, loss of about 36 %, auxiliary power devices, S2, D2 and D3, loss of about 14 %, DC reactor loss 22 % and the rest about 28 %.

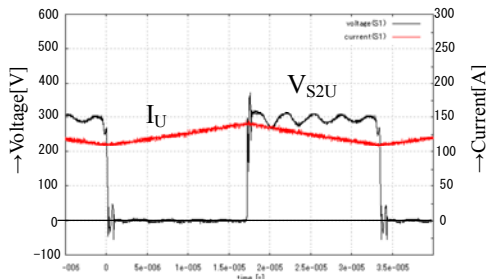


Figure 28: Voltage and current waveforms of the main switch S_{1U} (CM600DU-24NFH, 1200V, 600A), boost mode at 30 kHz-17kW, 145 V/291 V

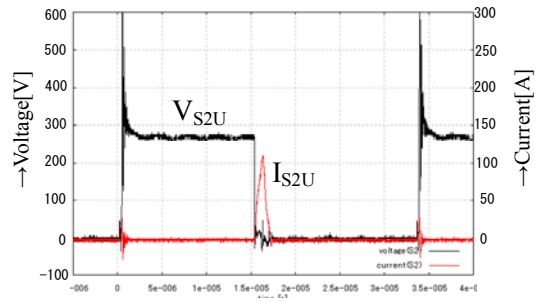


Figure 29: Voltage and current waveforms of the auxiliary switch S_{2U} (CM600DU-24NFH, 1200V, 600A), boost operation at 30 kHz-17 kW, 145 V/291 V

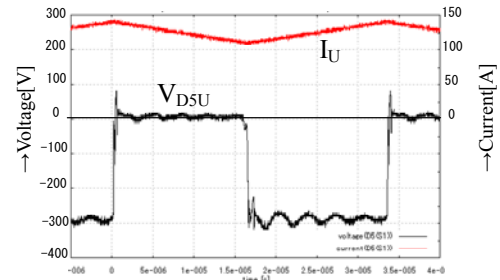


Figure 30: Voltage and current waveforms of the output diode D_{5U} (CM600DU-24NFH, 1200V, 600A), boost operation at 30 kHz-17 kW, 145 V/291 V

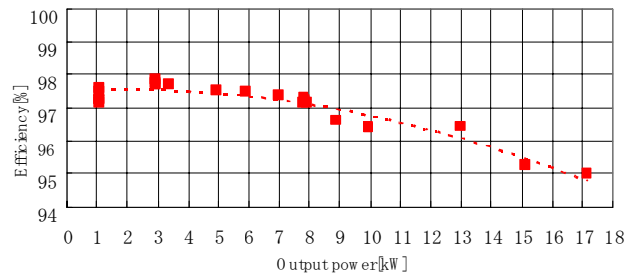


Figure 31: Efficiency of single phase in boost operation.

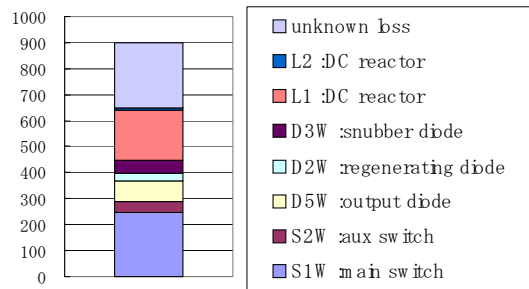


Figure 32: Loss breakdown for a single phase of the 3 phase SAZZ converter

III. HIGH POWER DENSITY

A power electronic converter is typically formed from the following main elements:

- Power Semiconductors
- Power Passives (Filters/Transformers)
- Interconnections
- Packaging elements
- Thermal management
- Control and auxiliary circuits

All of the elements contribute to the final converter power density and each of them must be considered in order to reach the highest power density possible. Because of the many elements, reaching a high power density is a complex process.

The root of the high power density is usually in high frequency operation and other factors can either support or invalidate its effects. As discussed in the paragraphs above, the high frequency operation can be attained via reducing losses in power semiconductors by employing soft switching converter topologies and advanced semiconductor devices. In the same time, passive components must be designed considering the high frequency operation with related power loss and heat production inside of the components. High power interconnections, packaging elements as well as thermal management assist the main power processing components in performing well close to their performance boundaries. Finally, control and auxiliary circuits control and monitor the converter performance and make sure that it operates as required by design specifications. Operation of all the elements close to the boundary is required in order to achieve the highest power density possible.

A. Contribution of Highly Efficient High Frequency Operation to Power Density

Highly efficient energy conversion has two main effects on the converter power density. The first effect relates to the possibility of increasing the operating frequency and hence reducing the volume of passive components. The second effect relates to the size of cooling system. High conversion efficiency reduces demands on the cooling capacity and hence the volume of the cooling system. Therefore, the high power density converter design should strive for reaching a balance between the volume of the cooling system and volume of the passive components. This is demonstrated in [7] for several components. As shown in Figure 33 for power transformer, power density curves usually exhibit an optimal operating frequency where power density is the highest. This relation is substantially altered by the addition of heatsinks and other components and therefore the final design must be the result of a complete system optimisation.

In addition to direct increase of operating frequency, the frequency can be increased also virtually by using interleaving of multiple phase shifted converter modules [28]. This approach splits the total output power into several portions which are individually processed by separate converter modules/phases. The phases operate phase-shifted with respect to each other which increases the operating frequency from the filtering point of view.

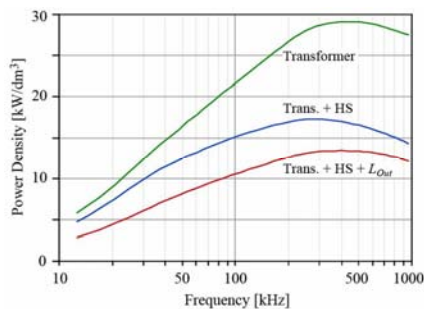


Figure 33: Example of power density of transformer with natural cooling (top line) with volume of semiconductors' heat sink added (middle) and volume of the output inductors added (bottom) [7]

In addition to this, the interleaving also reduces rms currents in the filter capacitors which results in further reduction of the filter volume. An optimisation of dc-dc converter from the number of phases point of view is discussed in [29]. As shown, interleaving has a positive effect on power density as well as on conversion efficiency. In the presented design, four interleaved phases offered the best results and were used in the prototype construction. Interleaved converters can use much more than four phases. A 1 kW converter with as many as 36 interleaved phases is presented in [30]. The presented designs resulted in improved efficiency and in the same time heatsinks could be completely omitted and the whole 1 kW converter could be constructed using solely SMD components.

B. Packaging for High Power Density

Packaging in power electronics has recently attracted a lot of attention. It has been recognised that proper classification of packaging terms [31] and quantification of packaging efficiency [32] can yield improvements in converter performance with respect to various design objectives. As demonstrated in [33], different approaches to packaging yield different results if evaluated from point of view of efficiency, power density, technological complexity, number of components, etc. From the power density point of view, all evaluated advanced concepts performed better than a design based on discrete components with higher than fourfold improvement in two presented cases.

According to [33], integration of components and increasing the functionality of packaging elements have large influence on power density. Increasing the functionality of packaging elements can be demonstrated on so called heat conductor converter [33] shown in Figure 34. In this design, copper bus-bar element fulfils functions of bus-bar, mechanical support, inductor winding and heat removal element in the same time. This substantially reduces the complexity of the converter design as well as the total converter volume due to using single element instead of four.

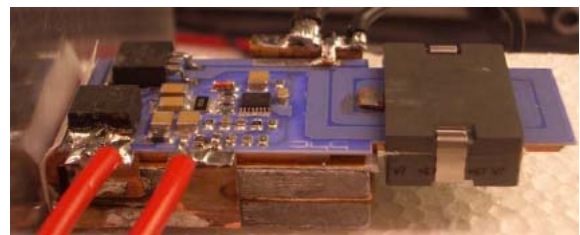


Figure 34: Heat conductor converter [33]

In integrated components, several devices utilise the same packaging as well as functional elements which reduces the total number of elements in the converter as well as their volume. The effect of this approach can be demonstrated for example on LLCT structure as presented in [34] where two inductors, a capacitor and a transformer are integrated into a single component. The resulting component requires only one set of heat removal and mechanically supporting elements which reduces the total volume. In the same time, air that would be present between the three components is largely rejected which further improves the power density.

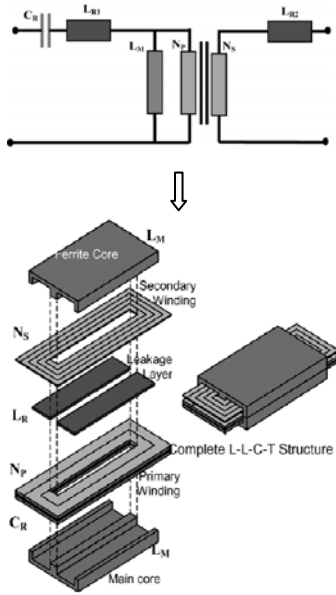


Figure 35: LLCT circuit diagram and internal structure [34]

C. Optimisation of Component Shapes and Layout

Addressing packaging in power converter design often results in using advanced technologies and materials. This is accepted in some applications but in some others a more conventional approach might be preferable due to cost limitations. As demonstrated in [35], truly high power density can be reached even by using solely conventional components by optimising the component shape and layout as well as paying close attention to the thermal management.

In conventional converter design, the largest space is usually wasted between the components due to their poor fitting or not paying attention to the geometrical component layout at all. In reality, any converter design offers certain flexibility to the component layout and increased effort can result in minimising the empty space inside the converter structure and hence in high power density. The flexibility in the design of passive components can help to mitigate the empty space as demonstrated in [36]. In the presented 50 kW converter design, transformer and inductor dimensions were chosen such that they would fit the dimensions of implemented IGBT modules. This resulted in little empty space inside the converter structure and in power density as high as 13 kW/l. Similarly in [35], diodes and capacitors are placed in the cavities next to the inductor winding (as shown in Figure 37 for diodes) which reduces the empty space and saves the extra space where these components would be placed otherwise.

D. Thermal Management and Power Density

A conventional way of removing heat from power components is by convection. In case of active components it often means individually cooled devices placed on heatsinks. In passive components it means airflow directly over components' surfaces. Convection has a big disadvantage with respect to power density which is the requirement of usually large empty spaces to allow for the required airflow. Therefore, in recent years conduction of heat away from passive as well as active components was introduced in power converters aiming for high power density. The use of conduction can be

demonstrated on examples shown in Figure 34, Figure 36 to Figure 38. The presented solutions range from using lead frame in relatively low power converters [38], thermal bus-bar [33], heatsink embedded components [39] to individually thermally solved components in high power converter [36]. All the presented solutions use relative simplicity and low volume of heat conducting elements. In the case of the solution presented in [36], the heat conduction is supported by using heat-pipes at critical places like for heat removal from transformer and inductor windings for example.

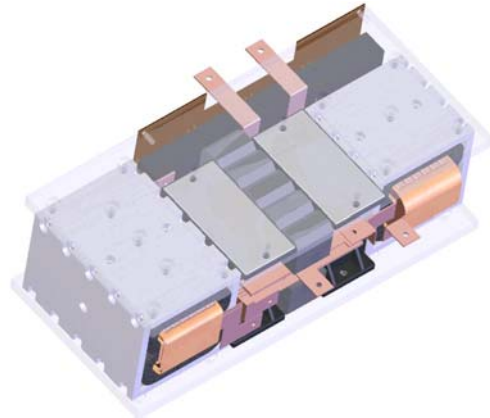


Figure 36: 50 kW converter with shape optimised components [36], [37]

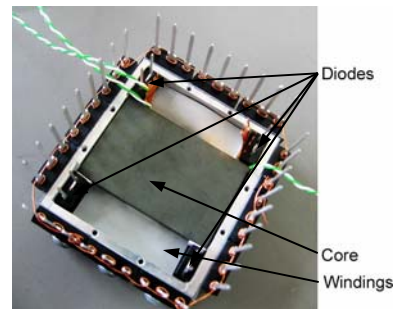


Figure 37: Placing components in winding cavities [35]

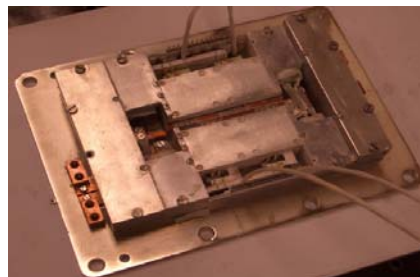
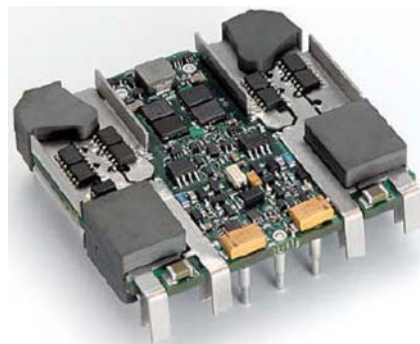


Figure 38: Heat removal based on lead frame [38] (top) and heatsink embedded components [39] (bottom)

E. Influence of Control and Auxiliary Circuits on Power Density

Little attention is usually paid to power density of control, gate drive and auxiliary circuits in conventional high power density converter designs. Their volume is considered small and “negligible” with respect to power processing circuits. The effectiveness of their design starts to play important role as the power density increases and at a certain point it becomes very critical. This can be demonstrated on the case study design as presented below. The power density of the complete converter can be as high as 25 kW/l for liquid-cooling but the power density of the gate drive circuit is only in the range of 0.3 – 0.5 kW/l. Because the gate drive circuit occupies almost 30 % of the converter volume, the power density of the power processing part is as high as 34 kW/l. In spite of the gate drives’ low power density, the gate drive design is rather advanced with the printed circuit board almost completely populated by components with vertical boards added to fit more components onto the restricted board area as can be seen in Figure 39. This means that the technology used for gate drive and control circuits becomes very important at really high power densities and improving power density of control and auxiliary circuits could substantially improve the power density of the complete converter.

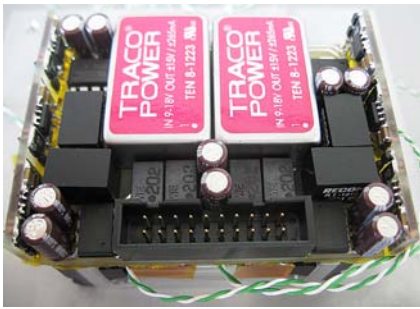


Figure 39: Gate drive unit of the case study converter

F. Overload Requirement and Power Density

Overload requirement in a converter design typically demands designing all power processing components for the overload power level and thermal management for the overload time duration. In the consequence, both these aspects result in a reduced power density if nominal power is considered due to the over-dimensioning of all components and thermal management parts. This is demonstrated on a simple example presented in Figure 40. The figure depicts the power density of the integrated inductor used in the design presented below at various power levels without considering the required thermal management. The two curves represent the design cases with and without the overload and the arrows indicate the power density reduction if the overload is required. The considered overload is 220 % in this case. The inductor volumes and consequently power densities are calculated by considering the saturation flux density as the core size limiting factor and the core winding gap as the winding size limit; thermal management is not considered. The cores used for this illustration are standard planar E cores as available in the core manufacturers’ catalogue.

As can be seen, power density of the inductor decreases as the output power increases. Even more substantial power density reduction is observed if the overload operation is required. The 220 % overload requirement

reduces the component power density to approximately 40 %. Further power density reduction can be expected in case if thermal management would be considered.

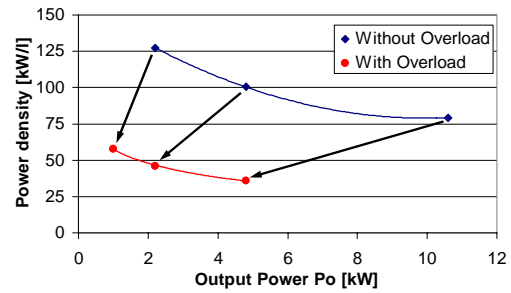


Figure 40. Power density for integrated SAZZ inductor with respect to converter output power, with and without overload requirement (overload 220 % considered)

The power density typically serves as a universal parameter for comparing different design approaches. The fact that it varies strongly with the overload requirement complicates the power density indication for such designs because the power density can be indicated without or with considering the overload. However, in both cases the resulting power density figures are not objective and therefore not comparable with the designs which do not require the overload operation. This occurs because in case of neglecting the overload requirement and considering only the nominal power, the resulting power density figure is very low and its reduction can be compared to what is indicated in Figure 40. Power density calculated in this way underestimates the converter design because all the power processing components must be designed for a higher power level required by the overload operation. On the other hand, if the overload is considered, the resulting power density is usually very high. This is unfair with respect to designs without the overload because converters designed for overload operation can not operate under overload conditions for an extended period of time (the thermal management is usually not designed to withstand such long overload operation). Therefore, in order to compare converter designs with and without the overload operation requirement, a new power density calculation methodology is needed.

The new methodology, first proposed in [40], is based on using maximal continuous power level to calculate the power density. This power level is typically higher than nominal because a thermal overhead is required in order to allow the overload operation. The new method removes the unfavourable conditions related to considering or not considering the overload operation. The resulting power density is higher than in case of using the nominal power level and lower than in the case of using the overload power level. Therefore, it is more realistic and fairer for comparison with designs which do not require the overload operation. Power density calculated in this way includes also the thermal management the design of which varies depending on the required overload time duration.

G. Converter Case Study with High Power Density, High Efficiency and Overload Capability

The main objectives of the presented design concept are high efficiency and power density. These objectives are followed by careful consideration of the issues addressed in the preceding discussion. As the result, following design choices are implemented in the converter design:

- Bidirectional SAZZ converter topology [41]
- Parallel CoolMOS devices – two parallel devices for main switches
- Integrated inductors
- Interleaved converter modules – four modules
- Conduction as the main heat removal method
- Layered converter structure with optimised space utilisation

More details on each design aspect can be found in [35].

1) Case Study Specifications

Main design specifications which are also considered as an example of specifications for traction automotive dc-dc converters are listed in Table IV. As can be seen, automotive converters must typically operate in a broad range of input and output voltages and they must also sustain a considerable overload (almost 240 % overload for the time period of 20 s in the presented case). Especially, the overload requirement has a great impact on the overall converter power density due to the necessity of designing all the components for the overload conditions.

TABLE IV.
MAIN CONVERTER SPECIFICATIONS

Input Voltage V_i [V]	120 – 166 ($V_{iN}=150V$)
Output Voltage V_o [V]	300 – 500 ($V_{oN}=300V$)
Output Power P_o [kW]	8.4 (20 kW overload for 20 s)
Operating Frequency f_s [kHz]	200

2) Converter Design

3D converter models are shown in Figure 41 though to Figure 44. Figure 41 and Figure 42 depict the single converter module in collapsed respectively exploded view. As can be seen from Figure 42, the structure is built around the integrated inductor positioned in the modules' centre. The interconnect PCB and Gate drive unit are positioned above the main converter body.

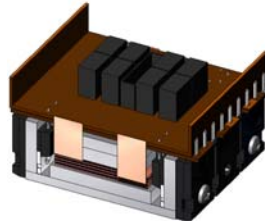


Figure 41. Single module collapsed view

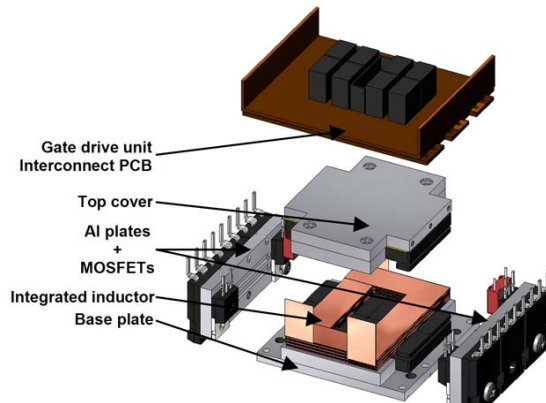


Figure 42. Single module exploded view

Figure 43 and Figure 44 show 3D models of the complete converter structure with air-cooling respectively liquid-cooling. The two structures are almost identical with the only difference being liquid cooled cold plate replaced by heat-pipes attached to forced air-cooled heatsinks in the case of the air-cooled assembly. Both structures are very compact and there is little empty space inside of them.

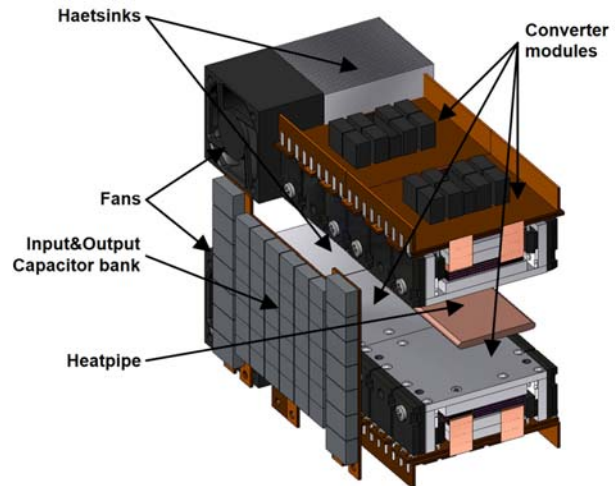


Figure 43. Complete air-cooled assembly

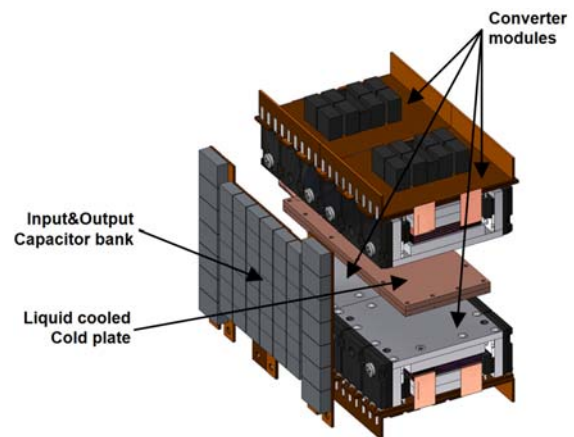


Figure 44. Complete liquid-cooled assembly

Figure 45 shows the prototype of the single 2.1 kW converter module next to an AA battery cell. As can be seen the converter module is very small and compact. The complete assembly of the liquid-cooled converter is then shown in Figure 46. Notice, there is little empty space available inside the converter structure.

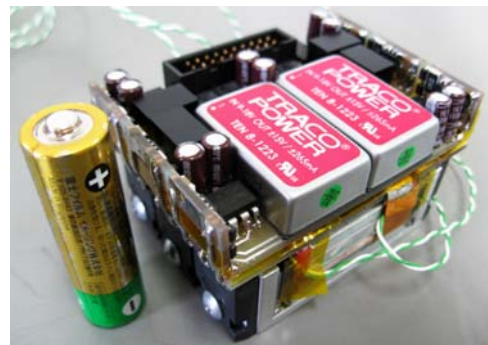


Figure 45: Single converter module prototype

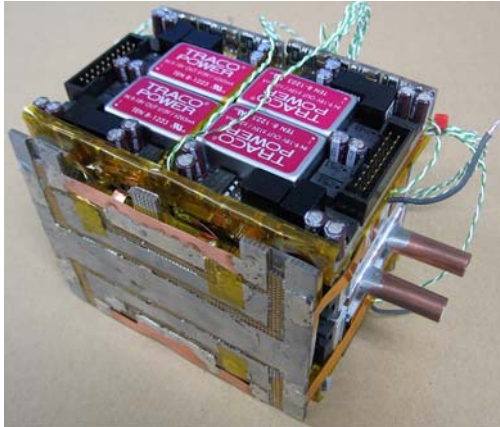


Figure 46: Complete liquid-cooled converter prototype

3) Experimental results

Tests performed on the single module converter prototype cover the complete range as required by the design specifications. Converter performance under continuous overload conditions was also tested in order to evaluate the converter power density using the approach as discussed in paragraph III.F. Test results performed on the complete converter were not available when writing this paper and therefore they are not included.

The complete efficiency curve for the power range from 600 W to approx 5 kW is shown in Figure 47. As can be seen the converter exhibits peak efficiency slightly higher than 95 % and this efficiency is held through the whole continuous overload power range up to 3.35 kW. The limit of continuous overload was determined by observing the temperature rise of the converters' top surface. Placing the thermocouples inside the converter structure was also considered but this could not be done due to the limited space. For the continuous power output of 3.35 kW, the measured temperature rise was 60 °C which was considered as the maximal allowed temperature rise. This value was chosen because it corresponds to a hot-spot in the inductor of approx. 150 °C for the heatsink temperature of 70 °C. Short-term overload was also tested under the temperature rise constrain of 60 °C. The time interval of 50 s was measured at the power output of 5 kW from the single module as the time required for the converters' top surface to heat-up by the specified temperature rise of 60 °C. This is much longer than the 20 s required by the design specifications. Notice that the converter efficiency is reduced to approximately 94 % under full overload of 5 kW which is still very high considering the overload of 240 %.

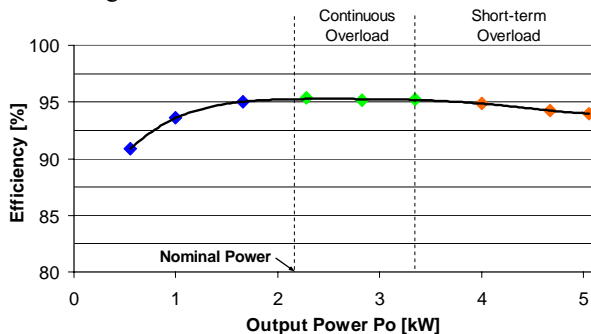


Figure 47. Efficiency curve of single module converter prototype with continuous as well as short-term overload, nominal voltage conversion 150 V to 300 V

Power density figures calculated by using different available power levels are listed in Table V. As discussed in paragraph III.F, the total power density of converters with overload operation should be calculated using the continuous overload power. Based on this assumption, the power density of the complete converter prototype was calculated as 25 kW/l for liquid cooling and 16.4 kW/l for air-cooling. These power densities are among the highest in the class.

TABLE V.
POWER DENSITIES CALCULATED FOR CONVERTER DESIGN II

	Nominal Power 8.4 kW	Continuous Overload 13.5 kW	Short-term Overload 20 kW
Power Density [kW/l]	Liquid-cooling		
	15.5	25	36
Power Density [kW/l]	Air-cooling		
	10.2	16.4	24.3

In case that bi-directional operation is not required, the output MosFETs can be replaced by conventional or SiC diodes. The possibility of using SiC diodes was tested in order to assess their influence on the converter efficiency. The comparison of efficiency curves measured with and without using SiC diodes is shown in Figure 48 for voltage conversion ratio of 120 V to 300 V. As can be seen, the efficiency improvement solely due to using SiC diodes is over 2 % in almost the whole considered power range. The peak efficiency under nominal voltage conversion of 150 V to 300 V was measured as high as 96.2 %. The final efficiency value could be still improved if measured on the complete converter with interleaved converter modules due to loss reduction in the input and output capacitors. Considering that the output MosFETs in the converter structure can be replaced by SiC diodes without any gain in converter volume, doing so would result in a power converter with power density of 25 kW/l and efficiency possibly as high as 97 %. This is a remarkable result considering that the whole converter is based solely on conventional components.

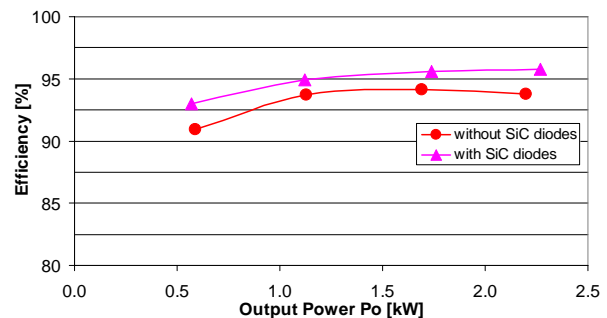


Figure 48. Comparison of efficiency curves of with and without SiC Diode in the rectifier, conversion 120 V to 300 V

IV. CONCLUSIONS

Vehicles with electric propulsion require highly efficient power converters with high power density. In this paper, issues related to reaching high power density and in the same time high efficiency are discussed. At first, several state of the art power converters based on SAZZ soft switching topology are presented. It is shown that efficiencies close to 98 % are attainable in high power converters at operating frequencies as high as 100 kHz using IGBT devices.

In the second part of the paper, issues related to reaching high power density in high power designs are discussed. It is pointed out that high power density is influenced by many design aspects and converters must be designed as close to the operational boundary as possible while most of the empty space inside of the converter structure should be eliminated in order to reaching as high power density as possible. It is also shown that the resulting power density is strongly dependent on the overload requirement and a new method of power density evaluation based on continuous overload is proposed. The discussed approach to high power density designs is concluded by presenting high power converter based on SAZZ topology and CoolMOS devices operating at 200 kHz. The presented prototype reaches power density as high as 25 kW/l while using only conventional components. In the same time, the conversion efficiency of the complete converter is expected to be as high 97 % based on the experimental results of a single converter module.

The presented design studies and converter prototypes are used in this paper as the proof of concept for reaching high power density and high efficiency. The presented results look promising but more studies are needed in order to improve the power density and conversion efficiency even further. The future efforts should concentrate on reaching conversion efficiencies beyond 99 % barrier while not harming the power density.

ACKNOWLEDGMENT

The authors would like to thank NEDO (New Energy Development Organisation, project ID: 05A48701d), JSPS (Japanese Society for Promotion of Science) and KAST(Kanagawa Academy of Science and Technology) for financially supporting the project.

REFERENCES

- [1] K.Shingo, K.Kaoru, T.Katsu, Y.Hata: "Development of Electric Motors for the TOYOTA Hybrid Vehicle "PRIUS"", EVS-17, Dec.2000
- [2] W.Yu, J.Lai, "Ultra High Efficiency Bidirectional DC-DC Converter With Multi-Frequency Pulse Width Modulation", APEC08, pp.1079-1084, 2008
- [3] A. Kawamura, Y.Tsuruta, S. Inasaka, " Proposal of electrical mileage for electric vehicle and discussions", IEEJ, VT-07-13, December 2007
- [4] Y. Ito, Y. Tsuruta, M. Bando, and A. Kawamura, "50kHz-25kW Bilateral Chopper Circuit SAZZ-1 for HEV", EVS-22, Oct.23-28, pp.848-857, 2006
- [5] H. Ohashi, "Recent Power Devices Trend (in Japanese)", Trans. of IEEJ, vol. 12, no.3, 2002, pp. 168-171.
- [6] H. Ohashi, "Power Electronics Innovation with Next Generation Advanced Power Devices", Proceeding of INTELEC'03, Oct. 2003, Yokohama (Japan), pp.9-13
- [7] J.W. Kolar, U. Drogenik, J. Biela, M.L. Heldwein, H. Ertl, T. Friedli, S.D. Round, "PWM Converter Power Density Barriers" Proceedings of Power Conversion Conference, PCC 2007, pp. 9 – 29, 2-5 April 2007
- [8] T. Teratani, "Vehicle Energy Management and Higher Voltage 42V for New Generation", 2nd International Congress on 42V Power Net(2000)
- [9] M.Okamura, E.Sato, S.Sasaki: "Development of Hybrid Electric Drive System Using a Boost Converter", EVS-20, Nov.2003
- [10] A.Kawamura, "Future commuter vehicles", KAST seminar on next generation mobility systems, 2007 November
- [11] S. Cuk and R.D. Middlebrook : "Advances on Switched-Mode Power Conversion Part I", *IEEE Trans. on Industrial Electronics*, Vol.IE-30, No.1, pp.10-19 (1983)
- [12] Richard G. Hoft : "Semiconductors Power Electronics", Van Nostrand Reinhold Company Inc. New York (1986) (in Japanese)
- [13] IEEJ : "Recent development on soft switching", IEEJ Technical Report, No.899, pp. 4-8 (2002-9)(in Japanese)
- [14] A. Kawamura : "Modern Power Electronics", SUURIKOUGAKU-SHA Co. Ltd., the First Edition, Tokyo, pp.39 (2005) (in Japanese)
- [15] G. Hua, C.S. Leu, and F.C. Lee : "Novel zero-voltage-transition PWM converters", *IEEE Trans. on Power Electronics*, Vol.9, NO.2, pp.213-219 (1994)
- [16] M.Nakamura, T.Myoui, M.Ishitobi, M.Nakaoka: "A Soft-Switching PWM Boost Chopper Controlled DC-DC Converter with A Single Passive Auxiliary Resonant Snubber and Its Performance Evaluations.", *T.IEE Japan*, Vol.122-D, No.10, pp.1006-1016, (2002)
- [17] Q. Zhao and F.C.Lee: "High-Efficiency, High Step-Up DC-DC Converters", *IEEE Trans. Power Electronics*, Vol.18, No.1, pp.65-73 (2003)
- [18] J.Zhang, R.-young Kim and J.-Sheng Lai: "High-Power Density Design of a Soft Switching High-Power Bidirectional DC-DC Converter", *Proc. of IEEE PESC06, WeA2-1*, pp.2119-2125 (2006)
- [19] K. Maikawa, Y. Tsuruta, and A. Kawamura: "Soft Switching Chopper Circuit for high power application", *IEEJ/JIASC 2003*, No.1-101, pp.477-478 (2003-8) (in Japanese)
- [20] Y. Tsuruta and A. Kawamura : "Proposed of 98.5% High Efficiency Chopper Circuit QRAS for the Electric Vehicle and the Verification", *T.IEE Japan*, Vol.125-D, No.11, pp.977-987 (2005) (in Japanese)
- [21] Y. Tsuruta, Y. Ito, and A. Kawamura : "The prompt report regarding the efficiency measurement of 8kW QRAS chopper using SiC schottky diode", *IEEJ/JIASC 2004*, No.1-85, pp.439-442 (2004) (in Japanese)
- [22] Y. Tsuruta, Y. Ito, and A. Kawamura : "8kW QRAS Chopper Using SiC Schottky Diode", *The 2005 International Power Electronics Conference, IPEC-Niigata 2005*, S30-3, pp.1113 – 1119 (2005)
- [23] Y. Tsuruta, Y. Ito, and A. Kawamura : "The proposal of SAZZ chopper circuit and test verification by means of the preceding fabrication", *2005 National Convention Record*, No.4-045, pp.71-72 (2005) (in Japanese)
- [24] Y. Tsuruta, Y. Ito, and A. Kawamura : "A High Frequency, High Efficiency and High Power Chopper SAZZ and the Test Evaluation at 100kHz-8kW", *IEEE 37th Annual Power Electronics Specialists Conference, PESC'06, WeA1-4*, pp.1965-1971 (2006)
- [25] Y. Tsuruta, Y. Ito, M. Bando, and A. Kawamura : "Proposal of Bilateral Buck and Boost Chopper Circuit SAZZ-1 for EV Drive Application and the Test Evaluation at 25kW", *IEEE International Conference on Industrial Technology, ICIT-2006, IF005878*, pp.1504-1509 (2006)
- [26] Y. Tsuruta and A. Kawamura : "Technical Stream on a High Efficiency and High Frequency Chopper Circuit", *IEEJ/JIASC 2006*, No. 1-o-6-2, pp. 1-139 – 1-144 (2006) (in Japanese)
- [27] Y. Tsuruta, M. Pavlovsky, and A. Kawamura : "Condition Limiting the Formation of the ZVZCT Switching in SAZZ Converter", *IEEE Industry Applications Conference 42nd Annual Meeting, IAS 2007*, IAS56p5, pp.1-6 (2007)
- [28] Chin Chang; M.A. Knights, "Interleaving technique in distributed power conversion systems", *IEEE Transactions on Circuits and Systems I: Fundamental Theory and Applications*, Volume 42 Issue 5, pp. 245 -251
- [29] M. Gerber, J.A. Ferreira, I.W. Hofsjajer, N. Seliger, "Interleaving optimization in synchronous rectified DC/DC converters", *Proceedings of Power Electronics Specialists Conference, PESC 2004, Achen – Germany*, pp. 4655 – 4661, Jun 2004
- [30] O. Garcia, P. Alou, J.A. Oliver, J.A. Cobos, " A high number of phases enables high frequency techniques and a better thermal management in medium power converters", *Proceedings of Conference on Integration of Power Electronics Systems, CIPS 2008*, pp. 281 – 284, March 2008
- [31] G.R. Blackwell, *The electronic packaging handbook*, Boca Raton CRC Press 2000

- [32] J. Popovic, J.A. Ferreira, "Concepts for high packaging and integration efficiency", Proceedings of Power Electronics Specialists Conference, PESC 2004, Volume 6, June 2004, pp. 4188 – 4194
- [33] J. Popovic, J.A. Ferreira, "Design and evaluation of highly integrated dc-dc converters for automotive applications", Proceedings of Industry Applications Conference, IAS 2005, Volume 2, Oct. 2005, pp. 1152 – 1159
- [34] J.T. Strydom, J.D. van Wyk, "Electromagnetic modeling for design and loss estimation of resonant integrated spiral planar power passives (ISP/sup 3/)", IEEE Transactions on Power Electronics, Volume 19, Issue 3, May 2004, pp. 603 – 617
- [35] M. Pavlovsky, Y. Tsuruta, A. Kawamura, "Automotive DC-DC converter designed for high power-density and high efficiency" Proceedings of Conference on Integration of Power Electronics Systems, CIPS 2008, pp. 191 – 195, March 2008
- [36] M. Pavlovsky, S.W.H. de Haan, J.A. Ferreira, "Concept of 50 kW DC/DC converter based on ZVS, quasi-ZCS topology and integrated thermal and electromagnetic design", European Conference on Power Electronics and Applications, EPE 2005, Sept. 2005
- [37] M. Pavlovsky, "Electronic DC transformer with High Power Density", PhD thesis Delft University of Technology, The Netherlands
- [38] J. Wanes, "A novel integrated packaging technique for high density DC-DC converters providing enhanced efficiency and thermal management", Proceeding of Applied Power Electronics Conference and Exposition, APEC 2004, Volume 2, pp. 1229 – 1235
- [39] M. Gerber, J.A. Ferreira, I.W. Hofsjager, N. Seliger, "High density packaging of the passive components in an automotive DC/DC converter", IEEE Transactions on Power Electronics, Volume 20, Issue 2, Mar 2005, pp. 268 – 275
- [40] M. Pavlovsky, Y. Tsuruta, A. Kawamura, "Pursuing High Power-Density and High Efficiency in DC-DC Converters for Automotive Application" Proceedings of Power Electronics Specialists Conference, PESC 2008, Jun 2008
- [41] Y. Tsuruta, M. Bando, Y. Ito and A. Kawamura, "A new circuit geometry SAZZ for an EV drive application", Proceedings of IEEE Industry Applications Conference, IAS 2006, pp.1-6